

See discussions, stats, and author profiles for this publication at: <https://www.researchgate.net/publication/264503781>

Fluorescent Properties Reinforced by Proton Transfer in the Salt 2,6 Diaminopyridinium Dihydrogen Phosphate

ARTICLE in THE JOURNAL OF PHYSICAL CHEMISTRY A · AUGUST 2014

Impact Factor: 2.69 · DOI: 10.1021/jp504343a

CITATIONS

2

READS

98

5 AUTHORS, INCLUDING:



Rajaboopathi Mani

9 PUBLICATIONS 35 CITATIONS

[SEE PROFILE](#)



Ivo B Rietveld

Université René Descartes - Paris 5

85 PUBLICATIONS 781 CITATIONS

[SEE PROFILE](#)



Marjatta Louhi-Kultanen

Lappeenranta University of Technology

84 PUBLICATIONS 780 CITATIONS

[SEE PROFILE](#)



Senthilkumar Muthu

Anna University, Chennai

2 PUBLICATIONS 2 CITATIONS

[SEE PROFILE](#)

Fluorescence Properties Reinforced by Proton Transfer in the Salt 2,6-Diaminopyridinium Dihydrogen Phosphate

Rajaboopathi Mani,[†] Ivo B. Rietveld,[‡] Krishnakumar Varadharajan,^{*,†} Marjatta Louhi-Kultanen,[§] and Senthilkumar Muthu[†]

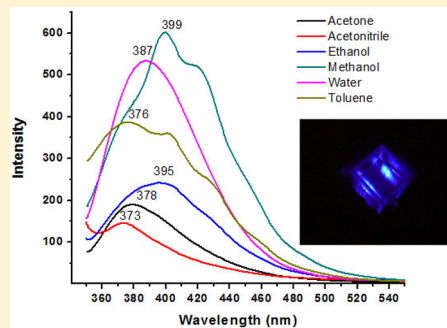
[†]Department of Physics, Periyar University, Salem 636 011, India

[‡]Laboratoire de Chimie Physique, Faculté de Pharmacie, Université Paris Descartes, 75006 Paris, France

[§]Department of Chemical Technology, Lappeenranta University of Technology, Lappeenranta 53851, Finland

S Supporting Information

ABSTRACT: Luminescent materials have many interesting applications, but it remains difficult to control the luminescence of organic materials and in particular to retain the same luminescence in solution and in the solid state, a property of interest for various imaging applications. In the present work, the fluorescent properties of the salt of 2,6-diaminopyridinium with dihydrogen phosphate have been explored. As a result of proton transfer from phosphoric acid to the pyridine nitrogen and the stabilizing effect of the two primary amines at the positions ortho to the pyridine nitrogen, the band gap between the HOMO and the LUMO is considerably diminished in comparison with that in 2,6-diaminopyridine. This is confirmed by a red shift in its absorption spectrum. Because protonation is retained in aqueous solution, the dissolved 2,6-diaminopyridinium dihydrogen phosphate salt retains a similar fluorescent spectrum as in the solid state. The crystals have been studied by single-crystal X-ray diffraction; FTIR, Raman, UV-vis-NIR, and luminescence spectroscopy; HOMO-LUMO calculations using DFT; and thermal analysis. The compound provides an example of a supramolecular motif that controls the crystal structure and the luminescence properties. In addition, the crystal exhibits negligible thermal expansion over a temperature interval of 150 °C. In short, 2,6-diaminopyridinium dihydrogen phosphate is an interesting compound for the design of luminescent devices.



1. INTRODUCTION

Systematic structural variation of luminescent organic molecules plays a vital role in crystal engineering for the enhancement of emission properties. Efficient emission of blue light from molecular crystals is less common than that of other colors in the visible spectrum,^{1–3} whereas it has great potential for applications in optoelectronic devices. Consequently, the molecular tailorability of promising molecules exhibiting this emission has received a great deal of attention.^{4–8} Despite challenges in obtaining emission at the appropriate wavelength, crystal engineers are continuously seeking effective ways to tune the luminescence properties by means of design and control over orientations, interactions, and stacking modes of molecules in the crystal structure.^{9–14}

1,4-Bis(4-cyanostyryl)benzene is a stilbene-type molecule that is arranged in a parallel manner with π - π stacking in the crystals. Its chromophore interaction distance is extended by cocrystal formation via halogen- and hydrogen-bonding interactions, and this enhances the emission properties of the crystals.¹³ Various arrangements of chromophores to enhance fluorescence emission in cocrystals have been achieved by selecting different conformers.¹³ A study of the improvement of the phosphorescence emission of crystalline organic compounds by the combined introduction of aromatic carbonyls,

heavy atoms, and halogen-bonding interactions has been conducted.⁸ Different anions such as H_2PO_4^- , F^- , Cl^- , Br^- , and I^- have been introduced to enhance the fluorescence properties of naphthalene derivatives.¹⁵ Additionally, specific aggregation of molecules with defined intermolecular interactions enhances the emission properties of organic crystals.^{10,16,17} For instance, the interplanar separation of many planar molecules in organic crystals is in the range 3.3–3.6 Å.¹⁸ Here this observation was taken as a guiding principle to tune the luminescence properties of 2,6-diaminopyridine (2,6-DAP) by combining it with phosphoric acid (Ph).

The crystal structure of pure 2,6-DAP exhibits a T-shaped interaction between two aromatic rings (see Figure 1S in the Supporting Information). In addition, N–H···N and N–H··· π hydrogen bonds interconnect the molecules in a zigzag fashion, leading to a complex three-dimensional (3D) network.¹⁹ This typical hydrogen-bonding interaction is observed in 2,6-DAP complexes with other molecules.^{20–24} Furthermore, the ability of the pyridine nitrogen to accept protons is high compared with the one substituted with an electron-donating amino

Received: May 3, 2014

Revised: July 25, 2014

group because of its strong basicity.²⁵ The anion precursor for the title salt is phosphoric acid, which has three hydrogen-bond donor sites and one hydrogen-bond acceptor site.

The binding energies for the different types of stacking of the pyridine rings in the gas phase have been calculated using electron correlation functions, and the antiparallel displaced packing is more stable (binding energy = 16.62 kJ/mol) than other geometries.²⁶ Crystal growth of the 2,6-DAP complex with picric acid has been studied, and its fluorescence spectrum has been reported.²⁷ Yu recently reported the crystal structure of the current system at 153 K.²⁸ Rietveld and co-workers compared the crystal structure of 3,4-diaminopyridinium dihydrogen phosphate (3,4-DAPPPh) with that of the hydrogen tartrate salt.²⁹ However, in the literature there is no detailed study explaining the structure–property relationships of 2,6-DAP-related compounds in relation to their luminescence.

Hence, this report discusses the synthesis, crystal growth, crystallographic observations, and supporting studies in relation to the fluorescence emission of the 2,6-DAPPPh salt. In addition, the molecular packing arrangement of 2,6-DAPPPh is compared with those of 2,6-DAP²⁸ and 3,4-DAPPPh.²⁹ The crystal structure of 2,6-DAPPPh at 293 K (CCDC 982445) is also reported.

2. EXPERIMENTAL SECTION

2.1. Crystal Growth. 2,6-DAP (1 M, 1.9 g) was dissolved in 30 mL of ethanol, and orthophosphoric acid (1 M, 0.57 mL) dissolved in 30 mL of ethanol was added to the 2,6-DAP solution. The reaction mixture was left to stir for 2 h at room temperature. A gray-colored precipitate formed, and it was washed several times with ethanol. The precipitate was dissolved in water, and a saturated solution was prepared for crystal growth. The solution was filtered using Whatman filter paper (cat. no. 1001 070). The filtrate was covered with perforated foil and allowed to evaporate slowly. Crystals were obtained after 10–14 days. Optically transparent single crystals of 2,6-DAPPPh were obtained after three recrystallizations in water. A picture of the 2,6-DAPPPh crystals is shown in Figure 1.

2.2. Characterization. X-ray diffraction data were collected on a Bruker Kappa APEX II single-crystal X-ray diffractometer. Mo $\text{K}\alpha$ radiation ($\lambda = 0.71073 \text{ \AA}$) with a graphite

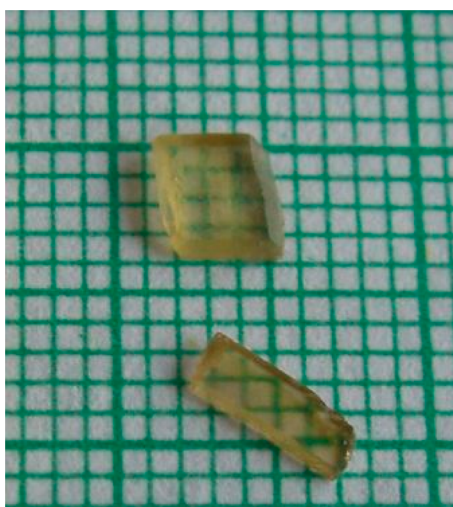


Figure 1. Photograph of 2,6-diaminopyridinium dihydrogen phosphate (2,6-DAPPPh) crystals.

monochromator in the incident beam was used. Data were reduced using SAINT/XPREP software (Bruker, 2004). Lorentz and polarization corrections were included. The absorption correction was performed by the multiscan method using SADABS (Bruker, 2004). All of the non-hydrogen atoms were found using a direct-method analysis in the SHELL-X-97 software.³⁰ After several cycles of refinement, the positions of the hydrogen atoms were calculated and added to the refinement process.

Intermolecular interactions of 2,6-DAP, 2,6-DAPPPh, and 3,4-DAPPPh were analyzed using Hirshfeld surfaces. The calculations were performed with Crystal Explorer³¹ using the experimental crystal geometries as input.^{28,29} Each point in the Hirshfeld surface corresponds to a (d_i , d_e) pair, where d_i and d_e denote the distances from the Hirshfeld surface to the nearest interior and exterior atom, respectively.³² The fingerprint plots of the interactions were obtained in the form of plots of d_i versus d_e .

The FTIR spectrum of the grown 2,6-DAPPPh crystal was recorded in KBr in the 400–4000 cm^{-1} wavenumber region using a Bruker Tensor 27 spectrometer at a resolution of 4 cm^{-1} . Absorption spectrum of 2,6-DAPPPh in aqueous solution were recorded on a PerkinElmer Lambda 25 spectrometer. The near-infrared (NIR) lower wavelength of 785 nm at 150 mW was selected for Raman measurements with a LabRam 300 Raman spectrometer equipped with a CCD detector from Horiba Jobin Yvon. The samples were irradiated for about 30 s to avoid fluorescence effects from the impurities. A PerkinElmer LS-45 fluorescence spectrometer was used to obtain the fluorescence spectrum with fixed slit width using a xenon lamp for UV light generation. The sample was excited at $\lambda = 335 \text{ nm}$. A spectrum was measured for a pellet sample of 2,6-DAPPPh mounted on a solid sample holder. Emission spectra of 2,6-DAPPPh in different solvents [ethanol, methanol, and water (polar protic); toluene (nonpolar); acetone and acetonitrile (polar aprotic)] were recorded.

Thermogravimetric and differential thermal analysis (TG/DTA) was performed on a NETZSCH STA 449 C instrument over the temperature range from 25 to 900 °C under a helium atmosphere at a flow rate of 70 mL/min and a heating rate of 10 K/min. A 10 mg sample of finely ground powder in an Al_2O_3 crucible was used for this measurement.

The optimized molecular structures of 2,6-DAP, 2,6-DAPPPh, and 3,4-DAPPPh in the ground state were computed by DFT using the B3LYP hybrid functional method and the 6-311+G(d,p) basis set to generate the HOMO–LUMO plots. The CIF files of these crystal structures were used for the optimization process.^{28,29}

3. RESULTS AND DISCUSSION

3.1. Molecular Arrangements. 2,6-DAPPPh crystallizes in the triclinic space group $P\bar{1}$ with lattice parameters $a = 7.4675(2) \text{ \AA}$, $b = 8.0924(2) \text{ \AA}$, $c = 8.1590(2) \text{ \AA}$, $\alpha = 70.8400(10)^\circ$, $\beta = 75.1150(10)^\circ$, and $\gamma = 84.936(2)^\circ$. The unit-cell volume at 293 K is $450.10(2) \text{ \AA}^3$ with $Z = 2$ formula units. The molecular structure of 2,6-DAPPPh from single-crystal X-ray analysis is shown in Figure 2. The crystallographic details and refinement parameters are presented in Table 1. The asymmetric unit consists of one protonated 2,6-diaminopyridinium cation ($2,6\text{-DAPH}^+$) and one dihydrogen phosphate anion (H_2PO_4^-). Since the unit-cell volume of this salt equals $452.77(3) \text{ \AA}^3$ at 150 K,²⁸ it is clear that its thermal expansion between 150 and 293 K is zero within experimental error. This

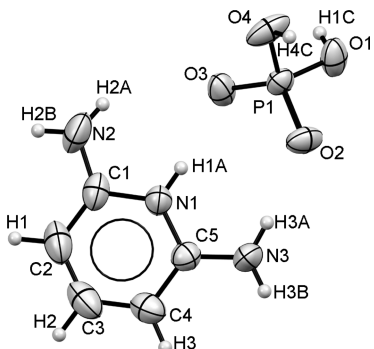


Figure 2. ORTEP plot (50% probability level) of 2,6-diaminopyridinium dihydrogen phosphate with atom numbering.

Table 1. Crystallographic Data for 2,6-Diaminopyridinium Dihydrogen Phosphate

empirical formula	C ₅ H ₁₀ N ₃ O ₄ P
crystal system	triclinic
space group	P $\bar{1}$
a/ \AA	7.4675(2)
b/ \AA	8.0924(2)
c/ \AA	8.1590(2)
α/deg	70.8400(10)
β/deg	75.1150(10)
γ/deg	84.936(2)
V/ \AA^3	450.10(2)
Z	2
$\rho_{\text{cal}}/\text{g cm}^{-3}$	1.528
absorption coefficient (μ)/mm ⁻¹	0.294
T/K	293(2)
$\lambda/\text{\AA}$	0.71073
reflections collected	7794
no. of parameters	216
goodness of fit	1.096
R indices	0.0303
wR ₂	0.0816
largest diff. peak, hole/e \AA^{-3}	0.264, -0.256

indicates that the intermolecular interactions in the crystal have to be strong. The proton transfer between phosphoric acid and 2,6-DAP is clearly revealed by an increase in the C–N–C bond angle and a reduced P–O distance in phosphoric acid.³³ More specifically, protonation of the N1 atom leads to an increase in the C1–N1–C5 angle [123.94(15) $^\circ$] with respect to the value found in the structure of neutral 2,6-DAP [118.6(3) $^\circ$].¹⁹ This is in line with the structures found in a search of the Cambridge Structural Database (CSD, version 5.35) in February 2014, for which structures with neutral 2,6-DAP molecules exhibit an average C1–N1–C5 angle of 117.7 $^\circ$ and structures containing 2,6-DAPH⁺ exhibit an average angle of 123.7 $^\circ$.³⁴ The same angle is 121.5(2) $^\circ$ for 3,4-DAPPPh, which also contains a protonated nitrogen atom in the pyridine ring.²⁹ The aromatic ring of the protonated 2,6-diaminopyridinium cation is planar. The distances and angles found in the experimental geometry of 2,6-DAPH⁺ are consistent with those found in the crystal structures of other 2,6-DAPH⁺ salts as determined by Mogul.^{34,35} In addition, the C–N bonds at the positions ortho to N1 are 1.344(3) \AA for N2 and 1.331(2) \AA for N3, respectively. These lengths are equivalent to those of the C–N bonds within the aromatic heterocycle, indicating that both nitrogen atoms are sp²-hybridized and stabilize the pyridinium

cation by sharing the electronic resonance in the π -deficient aromatic system. Their bond lengths are clearly shorter than for unprotonated 2,6-DAP, for which values of 1.347(4) \AA and 1.377(4) \AA were found for the primary amines.¹⁹ In the case of 3,4-DAPPPh, only the amine group at the para position is sp²-hybridized, indicating that the stabilization of the pyridinium cation is less efficient in this molecule.²⁹

The aromatic rings of neighboring 2,6-DAPH⁺ cations are involved in antiparallel $\pi\cdots\pi$ interactions (Figure 3; also see

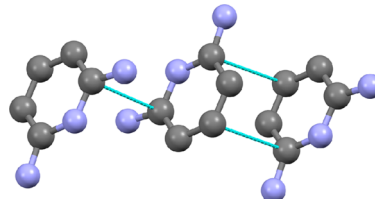


Figure 3. Antiparallel interaction of the 2,6-diaminopyridinium cations. Hydrogen atoms have been removed for clarity. The broken lines indicate the shortest distances between atoms on neighboring pyridine rings.

Figures 2S and 3S in the Supporting Information), with an interplanar distance of 3.44 \AA for the rings with mainly carbon–carbon interactions and one of 3.48 \AA for the carbon–primary amine (N2) interaction. $\pi\cdots\pi$ stacking of organic chromophores has given rise to intense fluorescence emission, as reported elsewhere,^{36–38} and the antiparallel stacking is reportedly the most stable for pyridine rings.²⁶ The distances in the present structure are slightly larger than the interplanar distance of 3.42 \AA between the rings in the structure of 3,4-DAPPPh, which also exhibits antiparallel $\pi\cdots\pi$ stacking;²⁹ on the other hand, parallel $\pi\cdots\pi$ interactions are absent in 2,6-DAP.¹⁹

Each cation possesses three strong N–H…O hydrogen bonds (Table 2), one forming a cyclic dimer [graph set

Table 2. Intermolecular Hydrogen Bonds in 2,6-DAPPPh

D–H…A	D…A distance/ \AA	D–H…A angle/ deg
N1–H1A…O3	2.748(2)	173.0(19)
N2–H2A…O3	3.233(2)	134(2)
N3–H3A…O2	2.905(2)	168(2)
N2–H2B…O1	3.070(2)	139(2)
N2–H2B…O2	3.339(2)	158.1(18)
C2–H1…O2	3.550(3)	136(2)
C3–H2…O1	3.470(2)	132.3(18)
N3–H3B…O4	2.951(2)	178(2)
O1–H1C…O3	2.563(3)	169.6(17)
O4–H4C…O2	2.528(2)	166.9(19)

assignment R₂²(8)] containing the proton on N1. The latter forms a strong hydrogen bond with a donor–acceptor distance of 2.748(2) \AA . The other hydrogen bond of the [R₂²(8)] cycle (N3–O2) has a donor–acceptor distance of 2.905(2) \AA . The third hydrogen bond linked to the cation, which also has N3 as the donor, is attached to another dihydrogen phosphate anion and has a length of 2.951(2) \AA ; its graph set is D (Figure 4). These structural features are very similar to those of 3,4-DAPPPh,²⁹ except for the position of the amino groups, which causes the hydrogen bonds to have a different overall orientation. In addition to the strong hydrogen bonds, moderate and weak ones are present in the structure too (Table 2). A moderate hydrogen bond with a donor–acceptor

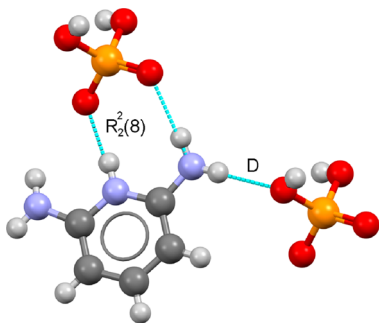


Figure 4. Strong hydrogen bonds connected to the DAP cation and graph sets of 2,6-DAPPPh. A similar configuration can be found for 3,4-DAPPPh.

distance 3.070(2) Å connects N2 with O1 of a dihydrogen phosphate anion from a third column. The latter phosphate anion is also linked by a weak hydrogen bond with N2 [3.339(2) Å], and another weak hydrogen bond with a length of 3.233(2) Å exists between O3, the acceptor of the N–H⁺ hydrogen bond, and H2A on N2.

Like that of 3,4-DAPPPh, the present structure possesses a complex 3D network consisting of intermolecular N–H···O hydrogen bonds between the organic cation and the surrounding dihydrogen phosphate anions. In addition, the phosphate ions are interconnected by O–H···O hydrogen bonds in exactly the same way as for the 3,4-DAPPPh structure.²⁹ The H₂PO₄[−] units form cyclic dimers [graph set R₂(8)] and infinite chains [graph set C(4)] propagating along the *b* axis. The O–H···O hydrogen bonds are very strong because the corresponding O···O distances [2.563(3) Å and 2.528(2) Å] are on the same order of magnitude as the O···O distance within the H₂PO₄[−] tetrahedron itself [about 2.51(2) Å]. Moreover, the short P···P distance [4.163(6) Å] along those chains indicates that the infinite chain can be considered as a single polyanion or macroanion with the graph set assignment (H₂PO₄)[∞]. These interactions give rise to a 3D supramolecular array of H₂PO₄[−] anion columns encapsulating the antiparallel π···π-stacked diaminopyridinium cations (Figure 5).

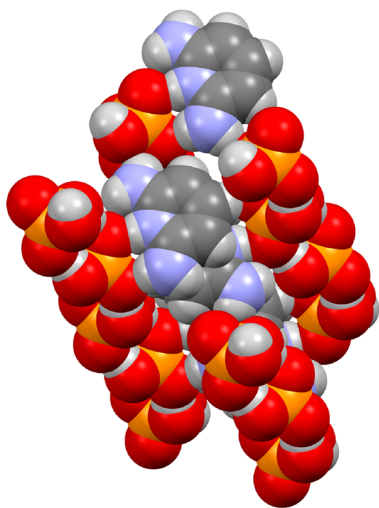


Figure 5. H₂PO₄[−] macroanion chains surrounding the antiparallel π-stacked 2,6-diaminopyridinium cations.

3.2. Fingerprint Plots. Hirshfeld fingerprint plots of 2,6-DAP, 2,6-DAPPPh, and 3,4-DAPPPh are presented in Figure 6. It

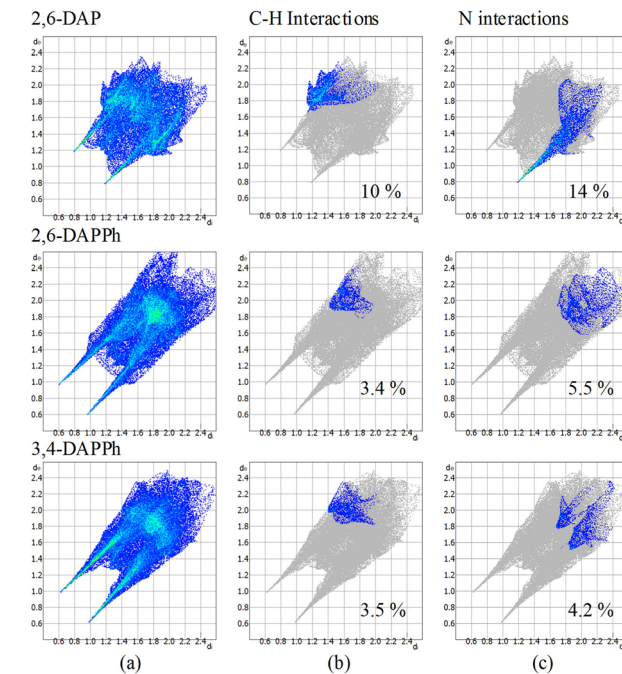


Figure 6. Fingerprint plots (d_e vs d_i) involving (a) all of the atoms of 2,6-DAP, 2,6-DAPPPh, and 3,4-DAPPPh; (b) the distances between the hydrogen atoms and the carbon atoms on the surrounding molecules; and (c) the distances between the nitrogen atoms and all of the other atoms on surrounding molecules. The percentages in comparison to all interactions (distances) have been provided.

can be seen that the compounds 2,6-DAPPPh and 3,4-DAPPPh have very strong hydrogen bonds (spikes to low d_i and d_e values), whereas 2,6-DAP has hydrogen bonds that are much less pronounced. Furthermore, the two structures containing dihydrogen phosphate have fairly similar interaction fingerprints, whereas 2,6-DAP clearly has a different interaction profile. 2,6-DAP has pyridine rings that are positioned perpendicular to each other with hydrogen atoms interacting with the π systems of the neighboring molecules, instead of the antiparallel stacked ring systems for the two systems containing dihydrogen phosphate. The C–H interactions in the 2,6-DAP structure are shorter than those in the two other structures and play a more important role in this structure, as can be seen in Figure 6. The interactions involving the N atoms are more important for the 2,6-DAP structure as a whole than in the other two cases. The nitrogen atom is an acceptor of hydrogen bonds in all three structures, but in the structures containing dihydrogen phosphate, these hydrogen bonds are weaker and oxygen on the phosphate is the acceptor for the strong hydrogen bonds. Figure 6 demonstrates that the structures of the salts of the 3,4-diaminopyridinium and 2,6-diaminopyridinium cations with dihydrogen phosphate are very similar, whereas the structure of 2,6-diaminopyridine is clearly different.

3.3. Vibrational Studies. The compound 2,6-DAP combines properties of both heterocyclic nitrogen and primary aromatic amines. The FTIR and Raman spectra of 2,6-DAPPPh are shown in Figures 7 and 8, respectively. Vibrational modes of the title crystal were assigned to different frequencies as presented in Table 3. These assignments were based on vibrational studies of 2,6-DAP and phosphoric acid.^{27,39–45}

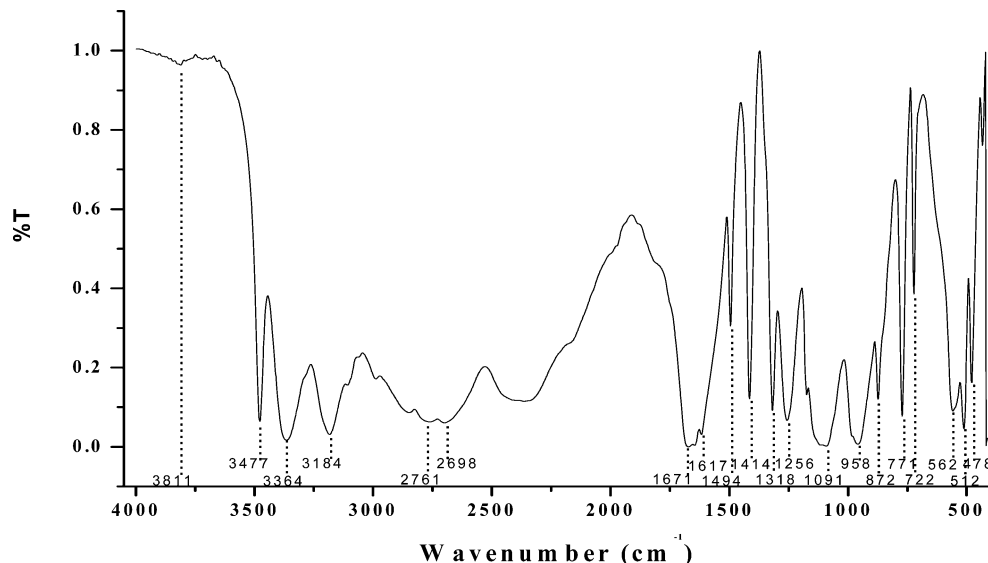


Figure 7. FTIR spectrum of solid 2,6-diaminopyridinium dihydrogen phosphate.

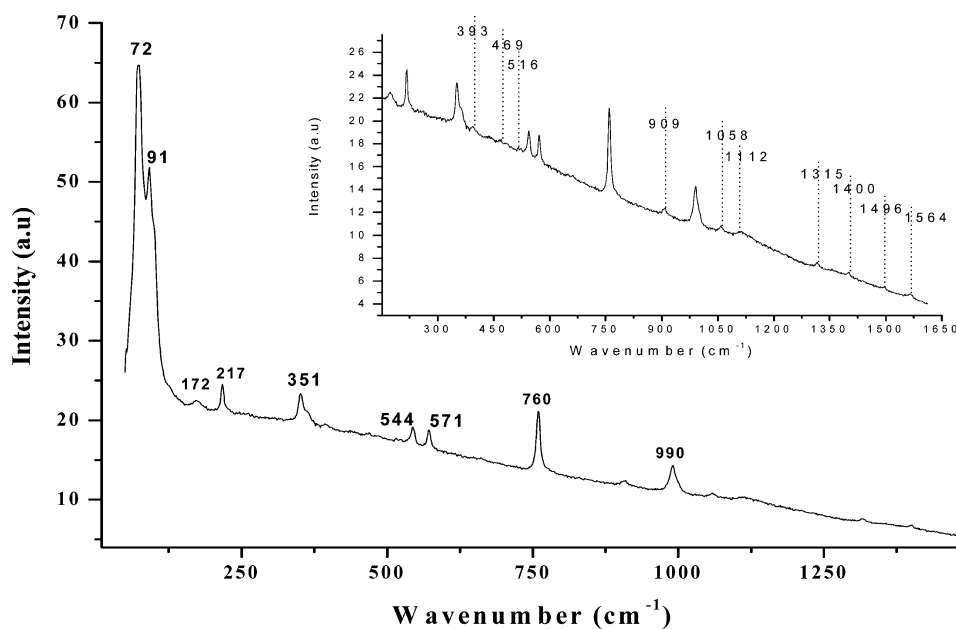


Figure 8. Raman spectrum of solid 2,6-diaminopyridinium dihydrogen phosphate. The inset shows weak bands.

Generally, hydrogen bonds can be identified by comparing vibrational frequencies of the functional groups that are involved in hydrogen-bond formation. Furthermore, the magnitude of the frequency shift reflects the strength of the hydrogen bond.^{46,47} In the title crystal, the N–H stretching frequency of the pyridinium salt was used as a probe to identify the proton displacement. The counterpart of the FTIR vibrations in the conjugated region of the molecules was observed using the Raman spectra. Both methods provide means to observe the presence of intermolecular and intramolecular interactions in the 2,6-DAPPh crystals.⁴⁸

In the FTIR spectrum, two strong bands at 3477 and 3364 cm^{-1} were assigned to NH_2 asymmetric stretching vibrations. The NH_2 symmetric stretching vibration was found as a broad, strong band at 3184 cm^{-1} . The band between 3150 and 3000 cm^{-1} can be ascribed to the C–H stretching vibration. This vibration is usually found in the region between 3100 and 3010

cm^{-1} .⁴⁹ The acid–base interaction involving the proton transfer gives rise to a hydrogen bond, and it appears as a broad and medium-strong band at 2698 cm^{-1} . Khan et al.²⁷ observed a similar band in this region for the salt of 2,6-DAP with picric acid. This band is due to the N–H⁺ stretching vibration of the pyridinium salt, occurring in the 3300–2370 cm^{-1} region.⁴⁹ A higher-frequency band between 1615 and 1575 cm^{-1} and a medium-intensity band between 1520 and 1465 cm^{-1} were assigned to C=C and N=H stretching vibrations, respectively. The NH₂ bending vibration was also observed at a higher frequency of 1564 cm^{-1} in the Raman spectrum. The C=C stretching vibration associated with the N–H bending vibration in the pyridine ring was assigned to the 1494 cm^{-1} band. It was ascribed to 1496 cm^{-1} in the Raman spectrum. The C=C and C=N stretching vibrations were observed at 1414 cm^{-1} . The N–H bending vibration was also found in this region. These vibrations show only very weak bands in the Raman spectrum.

Table 3. Vibrational Assignments of FTIR and Raman Spectra of 2,6-DAPP⁺

wavenumber (cm ⁻¹)	FTIR	Raman	assignment
3811 vw	—	$\nu(\text{OH})$	
3477 s	—	$\nu_{\text{asym}}(\text{NH}_2)$	
3364 s, b	—	$\nu_{\text{asym}}(\text{NH}_2)$	
3184 s, b	—	$\nu_{\text{sym}}(\text{NH}_2)$	
3108 m, s		$\nu(\text{C}-\text{H})$	
2985		$\nu(\text{C}-\text{H})$	
2761 ms	—		
2698 ms	—	N ⁺ –H hydrogen-bonded pyridinium salt	
1671 s, b	—	$\nu(\text{C}=\text{N})$	
1617 s, b	1564 vw	$\nu(\text{C}=\text{N}), \delta(\text{NH}_2)$	
1494 m	1496 vw	$\nu(\text{C}=\text{C}), \delta(\text{NH}_2)$	
1414 ms	1400 vw	$\nu(\text{C}=\text{C}), \delta(\text{NH}_2), \nu(\text{C}=\text{N})$	
1318 ms, n	1315 vw	C–H def vib, $\nu(\text{C}=\text{C})$	
1256 s	—	N–H def vib, C–H def vib	
1171		ring vibration	
1091 s, b	1058 w	$\nu_3(\text{PO}_4^{\text{-}})$	
—	990 ms	$\nu_1(\text{PO}_4^{\text{-}})$	
958 s	—	NH ₂ rocking, $\nu(\text{C}-\text{H})$	
—	909 w	$\nu(\text{P}-\text{OH})$	
872 s	830 vw	$\omega(\text{NH})$ out of plane	
771 s, sh	760 s, sh	$\beta(\text{C}=\text{C}-\text{C})$	
722 m, n	—	$\gamma(\text{C}-\text{H})$	
562 s	571 ms	C–C=C, C–N–C bending	
—	544 ms	C–C=C bending	
512 s	516 vw	$\nu_4(\text{PO}_4^{\text{-}})$	
478 s, sh	469 vw	$\gamma(\text{P}=\text{O})$	
—	393 vw	$\gamma(\text{N}-\text{H}), \gamma(\text{O}-\text{H})$	
—	351 ms	$\nu_2(\text{PO}_4^{\text{-}}), \rho(\text{C}-\text{NH}_2)$	
—	217 ms		
—	172 w	$\rho(\text{OH})$	
—	91 ms	$\rho(\text{P}=\text{O})$	
—	72 s	$\rho(\text{P}-\text{OH})$	

^aAbbreviations: vw, very weak; s, strong; ms, medium strong; m, medium; b, broad; sh, sharp; ν , stretching; ν_{sym} , symmetric stretching; ν_{asym} , asymmetric stretching; β , in-plane bending; γ , out-of-plane bending; ω , wagging; δ , scissoring; ρ , rocking

The medium-strong band at 1318 cm⁻¹ was assigned to C–H deformation vibrations. The strong band at 1256 cm⁻¹ was assigned to N–H deformation vibrations. However, usually this band occurs as a medium-weak band at 1250–1240 cm⁻¹ in the FTIR spectrum and as a medium band in the Raman spectrum.⁴⁹ The low-intensity band at 1171 cm⁻¹ was assigned to ring breathing vibrations. The observed variation in the N–H⁺ stretching vibration of the pyridine moiety and N–H deformation vibrations of the primary amines confirms the presence of strong interactions between 2,6-DAPP⁺ and the phosphoric acid anion.

The PO₄³⁻ anion is similar to the radical anions SO₄²⁻ and SeO₄²⁻, and its internal vibrations can be clearly observed by four modes: (1) the nondegenerate symmetric stretching mode ν_1 , (2) the doubly degenerate bending mode ν_2 , (3) the triply degenerate asymmetric stretching mode ν_3 , and (4) the triply degenerate asymmetric bending mode ν_4 in the FTIR and Raman spectra. The modes ν_1 and ν_3 involve symmetric and asymmetric stretching of the P–O bonds, whereas ν_2 and ν_4 involve mainly O–P–O symmetric and asymmetric bending. Panicker and co-workers performed a short review of these

vibrations for a range of phosphate complexes published previously.⁵⁰

These four internal vibrations occur at almost the same wavenumbers in the FTIR and Raman spectra.^{45–51} For the present system, these vibrations were observed at $\nu_1 = 990$ cm⁻¹, $\nu_2 = 351$ cm⁻¹, $\nu_3 = 1058$ cm⁻¹, and $\nu_4 = 515$ cm⁻¹ in the Raman spectrum. This is consistent with earlier reports.^{52,53} Comparison of the FTIR and Raman spectra clearly shows that the asymmetric modes (ν_3 and ν_4) are active in the IR spectra. The asymmetric stretching mode (ν_3) associated with the O–H out-of-plane bending vibration is observed at 1091 cm⁻¹ in the FTIR spectrum and occurs at 1058 cm⁻¹ in the Raman spectrum. The symmetric stretching mode (ν_1) was traced at 990 cm⁻¹ in the Raman spectrum but was not observed in the FTIR spectrum.

Furthermore, a strong peak at 958 cm⁻¹ in the FTIR spectrum was assigned to the ring breathing vibration. The N–H wagging vibration was traced as a strong band at 872 cm⁻¹ in the FTIR spectrum. This band was observed at 830 cm⁻¹ in the Raman spectrum. Ring bending vibrations (C–C=C and C–N–C) were assigned to the bands at 571 and 544 cm⁻¹ in the Raman spectrum and to the band at 562 cm⁻¹ in the FTIR spectrum. The asymmetric bending mode (ν_4) appears at 516 cm⁻¹ in the Raman spectrum. The bands at 469 cm⁻¹ in the Raman spectrum and 478 cm⁻¹ in the FTIR spectrum were assigned to the P=O out-of-plane bending vibration. The N–H and the O–H out-of-plane bending vibration was observed at 393 cm⁻¹ in the Raman spectrum. The symmetric bending mode (ν_2) appears at 351 cm⁻¹ in the Raman spectrum. The C–NH₂ rocking mode was also associated with the symmetric bending mode ν_2 . The bands at 217 and 172 cm⁻¹ in the Raman spectrum were assigned to the O–H rocking mode. The phosphoric acid vibrations at lower wavenumbers, which were not observed in the FTIR spectrum, were clearly present in the Raman spectrum. Thus, the vibrations observed by FTIR related to the pyridine ring system at 1494, 1414, 1318, 771, and 571 cm⁻¹ have their Raman counterparts at 1496, 1400, 1315, 760, and 562 cm⁻¹.⁵⁴

3.4. UV–Vis–NIR Studies. The UV–vis–NIR spectrum of 2,6-DAPP⁺ measured in aqueous solution is presented in Figure 9. It exhibits two absorption peaks at 240 and 330 nm

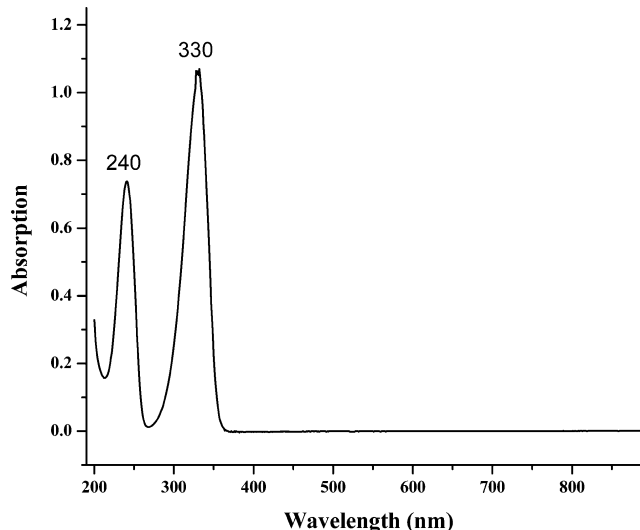


Figure 9. Absorption spectrum of 2,6-DAPP⁺ in aqueous solution.

for the $n-\pi^*$ - and $\pi-\pi^*$ -type transitions, respectively, induced by the UV light irradiation.⁵³ The absorption peaks of 2,6-DAP in methanol were found to be at 245 and 309 nm.⁵⁵ The observed 21 nm red shift in λ_{max} in water relative to methanol is due to changes in the π -electron density in the primary amine groups and the pyridine nitrogen in the ground state. Additionally, stronger dipole–dipole interactions between the polar solvent and the molecule stabilize the excited state. On the other hand, the blue shift of the peaks resulting from the $n-\pi^*$ transition is due to increased solvation of the lone pair in the ground state, which lowers the energy of the n orbital, thereby increasing the energy gap between the n and π^* orbitals. This effect dominates the interaction of the primary amines with solvent molecules.⁵⁶

3.5. Fluorescence Studies. The emission wavelength effectively depends on the HOMO–LUMO gap associated with charge transfer within the diaminopyridine moiety. This property has been studied for the 2,6-DAP molecule in different solvents at various pH values, and the observed peak shifts have been explained by the interaction of solvent molecules with (1) the lone pairs of the amine groups, (2) their hydrogen atoms, and (3) the pyridine-ring nitrogen.³⁹ In the solid state, the emission wavelength depends on factors such as $\pi-\pi$ interactions resulting from molecular packing, distances between interacting π systems, and their angles.¹¹ The solid-state emission spectrum of 2,6-DAPPPh is shown in Figure 10. The emission spectra of 2,6-DAPPPh in different solvents are presented in Figure 11.

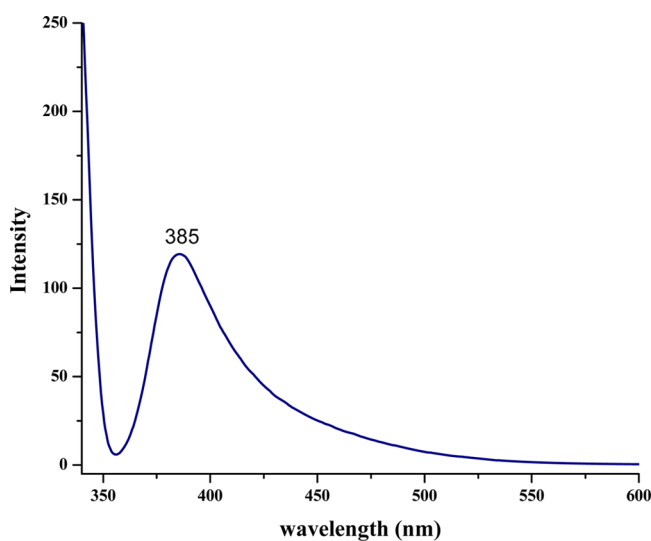


Figure 10. Fluorescence spectrum of solid 2,6-DAPPPh.

In comparison with the solid-state emission spectrum (385 nm), red and blue shifts are observed for polar protic and for nonpolar or polar aprotic solvents, respectively. The observed shifts in the emission spectra of 2,6-DAPPPh in different solvents are consistent with intramolecular charge transfer involving the primary amines and proton transfer between phosphoric acid and the pyridine ring in addition to solute–solvent interactions. Furthermore, the charge transfer is evidenced by the large Stokes shift (the difference between the wavelengths of the band maxima in the absorption and emission spectra). The red shift in the emission in solution is due to the interaction of the solvent with the hydrogens on the primary amines and the pyridine nitrogen. The blue shift results from interactions of

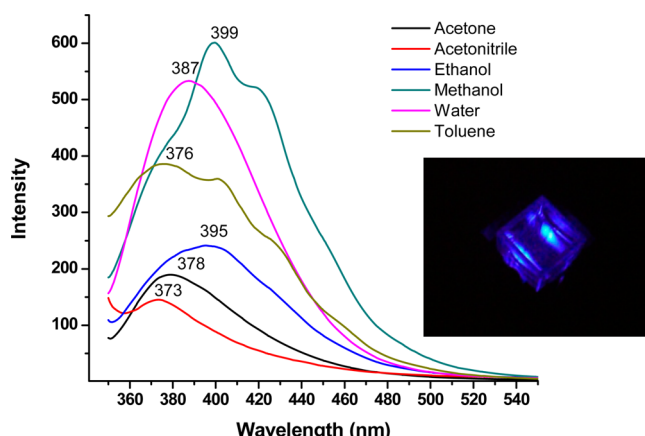


Figure 11. Fluorescence spectra of 2,6-DAPPPh in different solvents. The inset shows a photograph of its fluorescence in aqueous solution while its spectrum was recorded.

solvent molecules with the lone pairs on the nitrogen atoms.³⁹ The blue-color emission maximum, $\lambda_{\text{max}} = 387$ nm, for 2,6-DAPPPh in water is very close to the maximum wavelength observed for the solid-state emission spectrum. Similar emission maxima in the solid state and in solution are not often observed for fluorescent materials^{57,58} and can be an advantage for applications. The decrease in emission intensity in polar aprotic solvents is due to a decrease in the energy difference between the states of the $n-\pi^*$ and $\pi-\pi^*$ transitions, which leads to increased vibronic decay between the solvent and 2,6-DAPPH⁺.^{2,39}

Representations of the HOMO and LUMO contours of 2,6-DAP, 2,6-DAPPPh, and 3,4-DAPPPh in the gas phase are shown in Figure 12, and the energy levels are given in Table 4. The HOMO energies of all the systems are lower than the LUMO energies. Furthermore, it can be seen in Figure 12 that the position of the HOMO of the 2,6-DAP molecule is the same in both structures. The electron density for protonated 3,4-DAP is different in the ground state, and its energy is even lower.

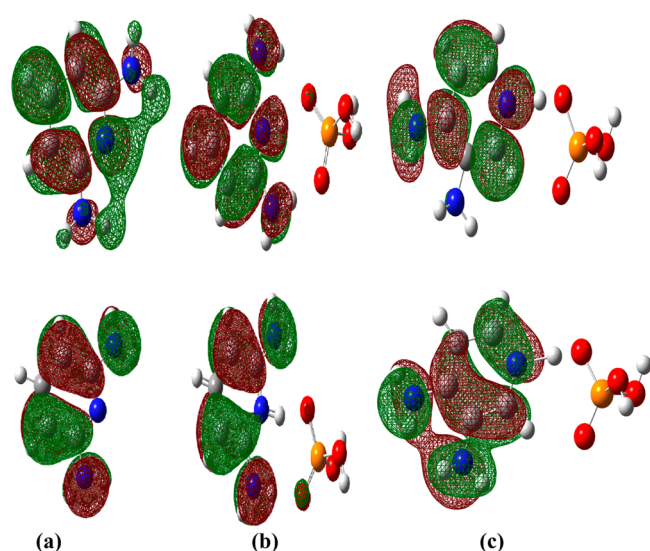


Figure 12. (bottom) Highest occupied and (top) lowest unoccupied molecular orbitals of (a) 2,6-DAP, (b) 2,6-DAPPPh, and (c) 3,4-DAPPPh in the gas phase. The molecular orbital wave functions are positive in the red regions and negative in the green regions.

Table 4. Calculated HOMO and LUMO Energies in the Gas Phase for 2,6-DAP, 2,6-DAPPPh, and 3,4-DAPPPh

molecule	E_{HOMO} (eV)	E_{LUMO} (eV)	ΔE (eV)
2,6-DAP	-5.46	-0.32	5.14
2,6-DAPPPh	-6.20	-1.49	4.71
3,4-DAPPPh	-6.34	-1.03	5.31

Interestingly, the difference in the location of the amine groups has a strong effect on the energy of the LUMO: that of 2,6-DAP with Ph is considerably lower than that of 3,4-DAP with Ph, and it can also be seen that the sp^3 amine group of 3,4-DAP at the position meta to the pyridine nitrogen does not participate in the LUMO. The diminished stabilization in combination with a strongly stabilized HOMO gives rise to a larger band gap for 3,4-DAP with phosphate than for 2,6-DAP alone. On the other hand, the band gap for 2,6-DAP with Ph is decreased considerably in comparison with that for pure 2,6-DAP. It is therefore clear that protonation of the pyridine nitrogen decreases the energy of the HOMO, as has also been reported in literature,⁹ but it is the additional stabilization by both primary amines at the ortho positions that significantly decreases the band gap between the HOMO and the LUMO. The red shift observed in the fluorescence spectrum for 2,6-DAPPPh ($\lambda_{\text{max}} = 365 \text{ nm}$ for 2,6-DAP in water³⁹) confirms the low value of its HOMO–LUMO energy gap.^{9,59}

3.6. Thermal Analysis. The TG/DTA plot of 2,6-DAPPPh is presented in Figure 13. The onset temperature of the melting

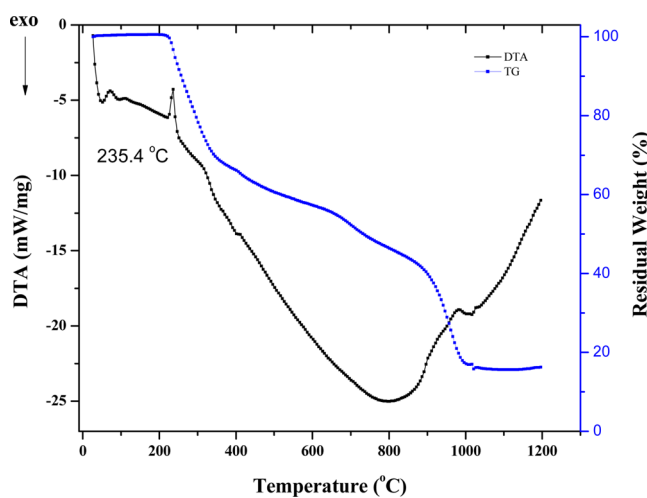


Figure 13. Thermogravimetric (blue, right-hand axis) and differential thermal analysis (black, left-hand axis) plot for 2,6-DAPPPh.

peak was found to be about 227 °C in the DTA curve. No mass loss was observed before the onset temperature in the TGA measurement, but a pronounced decrease started at 228 °C. This indicates that no volatile impurities or water were present in the crystals. However, the compound started to decompose just after the onset of melting. The decomposition was completed in four stages, in which the sample lost 28%, 16%, 15%, and 24% of its weight. A glassy white ash residue of 16% was observed after the measurements.⁶⁰

4. CONCLUSIONS

2,6-Diaminopyridinium dihydrogen phosphate was obtained by slow evaporation from aqueous solution. Crystal structure analysis revealed that intermolecular packing consists of long

molecular chains formed by dihydrogen phosphate anions interconnected with O–H···O hydrogen bonds along the *c* axis direction. The pyridinium cations are organized in columns through antiparallel π – π interactions. These π -stacked columns are surrounded by infinite molecular chains of dihydrogen phosphate. The anions and cations are interconnected by N–H···O hydrogen bonds. The structure of 2,6-DAPPPh is very similar to that of 3,4-DAPPPh, with similar hydrogen-bonding interactions and similar π stacking; in the crystal structure of pure 2,6-DAP, however, antiparallel π stacking is absent and replaced by T-shaped π ··· π interactions without any stacking. Fingerprint plots based on Hirshfeld surfaces demonstrate that the hydrogen-bonding interactions in 2,6-DAPPPh are much stronger than in 2,6-DAP because of the presence of the phosphate ion. Moreover, the most important difference is the protonation of the pyridine nitrogen atom by the phosphoric acid, which is observed for the structures of 2,6-DAPPPh and 3,4-DAPPPh and completely absent in 2,6-DAP. The differences between the two structures of 2,6-DAPPPh and 3,4-DAPPPh mainly concern the manner in which the position of the external primary nitrogen atoms modifies the orientation of the hydrogen bonds. In addition, both of the primary nitrogen atoms are clearly sp^2 -hybridized for 2,6-DAPPPh. This increases the stabilization of the N1 protonation in the pyridine ring and lowers the energy levels involved in the phosphorescence decay, in particular that of the excited state. The observed variation of the pyridine N–H⁺ stretching and primary amine N–H deformation bands for the molecular vibrations confirms the proton transfer from phosphoric acid to 2,6-diaminopyridine.

The red shift observed in the emission spectrum of dissolved 2,6-DAPPPh in polar protic solvents (water) versus polar aprotic solvents (methanol) is due to the solvent–solute interactions and the intramolecular charge transfer facilitated by the protonation of the DAP moiety affecting the π – π^* transition in 2,6-DAPPPh, which is responsible for its fluorescence. The HOMO–LUMO energy gaps calculated for 2,6-DAP and 2,6-DAPPPh in the gas phase are 5.14 and 4.71 eV, respectively. This band gap decrease is confirmed by the red shift observed in the emission spectrum of 2,6-DAPPPh compared with 2,6-DAP. The fluorescence spectra of 2,6-DAPPPh in the solid state and in water are very similar, and in addition, the crystal structure does not exhibit any significant thermal expansion. Therefore, it may be a useful compound for imaging and other applications.

ASSOCIATED CONTENT

S Supporting Information

A figure showing the packing of 2,6-DAP, presenting the cross-linking of molecules through N–H···N and N–H··· π interactions; two figures showing the packing of 2,6-DAPPPh, one displaying the stacking of DAP molecules viewed down the crystallographic *c* axis and the other displaying the stacking of DAP molecules (space-filling model) viewed down the crystallographic *b* axis. This material is available free of charge via the Internet at <http://pubs.acs.org>.

AUTHOR INFORMATION

Corresponding Author

*E-mail: vkrishna_kumar@yahoo.com. Phone: +91 427-2345766, ext. 246. Fax: +91 427-2345565.

Notes

The authors declare no competing financial interest.

ACKNOWLEDGMENTS

The authors thank SAIF (IIT Madras) for single-crystal X-ray diffraction measurements. R.M. thanks Prof. T. N. Guru Row and Dr. Amol G. Dikundwar (Solid State and Structural Chemistry Unit, Indian Institute of Science, Bangalore) for fruitful discussions and their interest in this work.

REFERENCES

- (1) Zhang, Z.; Zhang, Y.; Yao, D.; Bi, H.; Javed, I.; Fan, Y.; Zhang, H.; Wang, Y. Anthracene-Arrangement-Dependent Emissions of Crystals of 9-Anthrylpyrazole Derivatives. *J. Am. Chem. Soc.* **2009**, *131*, 5069–5076.
- (2) Wu, K. C.; Ku, P. J.; Lin, C. S.; Shih, H. T.; Wu, F. I.; Huang, M. J.; Lin, J. J.; Chen, I. C.; Cheng, C. H. The Photophysical Properties of Diphenylbenzenes and their Application as Exceedingly Efficient Blue Emitters for Electroluminescent Devices. *Adv. Funct. Mater.* **2008**, *18*, 67–75.
- (3) Wei, Y.; Chen, C. T. Doubly Ortho-Linked *cis*-4,4'-Bis(diarylaminostilbene/Fluorene Hybrids as Efficient Nondoped, Sky-Blue Fluorescent Materials for Optoelectronic Applications. *J. Am. Chem. Soc.* **2007**, *129*, 7478–7479.
- (4) Friend, R. H.; Gymer, R. W.; Holmes, A. B.; Burroughes, J. H.; Marks, R. N.; Taliani, C.; Bradley, D. D. C.; Dos Santos, D. A.; Brédas, J. L.; Lögdlund, M.; Salaneck, W. R. Electroluminescence in Conjugated Polymers. *Nature* **1999**, *397*, 121–128.
- (5) Schmidtke, J.; Stille, W.; Finkelmann, H.; Kim, S. T. Laser Emission in a Dye Doped Cholesteric Polymer Network. *Adv. Mater.* **2002**, *14*, 746–749.
- (6) Gao, F.; Liao, Q.; Xu, Z.; Yue, Y.; Wang, Q.; Zhang, H.; Fu, H. Strong Two-Photon Excited Fluorescence and Stimulated Emission from an Organic Single Crystal of an Oligo(phenylene vinylene). *Angew. Chem., Int. Ed.* **2010**, *49*, 732–735.
- (7) Muthuraman, M.; Masse, R.; Nicoud, J. F.; Desiraju, G. R. Molecular Complexation as a Design Tool in the Crystal Engineering of Noncentrosymmetric Structures. Ideal Orientation of Chromophores Linked by O–H···O and C–H···O Hydrogen Bonds for Nonlinear Optics. *Chem. Mater.* **2001**, *13*, 1473–1479.
- (8) Bolton, O.; Lee, K.; Kim, H. J.; Lin, K. Y.; Kim, J. Activating Efficient Phosphorescence from Purely Organic Materials by Crystal Design. *Nat. Chem.* **2011**, *3*, 205–210.
- (9) Zhang, H.; Wan, X.; Xue, X.; Li, Y.; Yu, A.; Chen, Y. Selective Tuning of the HOMO–LUMO Gap of Carbazole-Based Donor–Acceptor–Donor Compounds toward Different Emission Colors. *Eur. J. Org. Chem.* **2010**, *1681–1687*.
- (10) Xie, Z.; Wang, H.; Li, F.; Xie, W.; Liu, L.; Yang, B.; Ye, L.; Ma, Y. Crystal Structure of a Highly Luminescent Slice Crystal Grown in the Vapor Phase: A New Polymorph of 2,5-Diphenyl-1,4-Distyrylbenzene. *J. Am. Chem. Soc.* **2007**, *129*, 2512–2516.
- (11) Chandaluri, Ch. G.; Radhakrishnan, T. P. Zwitterionic Diaminodicyanoquinodimethanes with Enhanced Blue-Green Emission in the Solid State. *Opt. Mater.* **2011**, *34*, 119–125.
- (12) Itoh, T. Fluorescence and Phosphorescence from Higher Excited States of Organic Molecules. *Chem. Rev.* **2012**, *112*, 4541–4568.
- (13) Yan, D.; Delori, A.; Lloyd, G. O.; Friscic, T.; Day, G. M.; Jones, W.; Lu, J.; Wei, M.; Evans, D. G.; Duan, X. A Cocrystal Strategy To Tune the Luminescent Properties of Stilbene-Type Organic Solid-State Materials. *Angew. Chem., Int. Ed.* **2011**, *50*, 12483–12486.
- (14) Sonoda, Y.; Goto, M.; Tsuzuki, S.; Tamaoki, N. Fluorinated Diphenylpolyenes: Crystal Structures and Emission Properties. *J. Phys. Chem. A* **2007**, *111*, 13441–13451.
- (15) Zhang, B. G.; Xu, J.; Zhao, Y. G.; Duan, C. Y.; Cao, X.; Meng, Q. J. Host–Guest Complexation of a Fluorescent and Electrochemical Chemsensor for Fluoride Anion. *Dalton Trans.* **2006**, *1271–1276*.
- (16) An, B. K.; Kwon, S. K.; Jung, S. D.; Park, S. Y. Enhanced Emission and its Switching in Fluorescent Organic Nanoparticles. *J. Am. Chem. Soc.* **2002**, *124*, 14410–14415.
- (17) An, B. K.; Lee, D. S.; Lee, J. S.; Park, Y. S.; Song, H. S.; Park, S. Y. Strongly Fluorescent Organogel System Comprising Fibrillar Self-Assembly of a Trifluoromethyl-Based Cyanostilbene Derivative. *J. Am. Chem. Soc.* **2004**, *126*, 10232–10233.
- (18) Dahl, T. The Nature of Stacking Interactions between Organic Molecules Elucidated by Analysis of Crystal Structure. *Acta Chem. Scand.* **1994**, *48*, 95–106.
- (19) Schwalbe, C. H.; Williams, G. J. B.; Koetzle, T. F. A Neutron Diffraction Study of 2,6-Diaminopyridine at 20 K. *Acta Crystallogr., Sect. C* **1987**, *43*, 2191–2195.
- (20) Al-Dajani, T. M.; Talaat, J.; Shamsuddin, S.; Hemamalini, M.; Fun, H. K. Bis(2,6-diaminopyridinium)bis(hydrogen oxalate) Monohydrate. *Acta Crystallogr., Sect. E* **2011**, *67*, o591–o592.
- (21) Al-Dajani, T. M.; Abdallah, H. H.; Mohamed, N.; Rosli, M. M.; Fun, H. K. 2,6-Diaminopyridinium 2-Carboxybenzoate. *Acta Crystallogr., Sect. E* **2010**, *66*, o2433–o2434.
- (22) Haddad, S. F.; Al-Far, R. H. 2,6-Diaminopyridinium Bromide Monohydrate. *Acta Crystallogr., Sect. E* **2003**, *59*, o1444–o1446.
- (23) Aghabozorg, H.; Saei, A. A.; Ramezanipour, F. 2,6-Diaminopyridinium Pyridinium-2,6-Dicarboxylate: A Redetermination. *Acta Crystallogr., Sect. E* **2005**, *61*, o3242–o3244.
- (24) Buyukgungor, O.; Odabasoglu, M. 2,6-Diaminopyridinium Hydrogen Fumarate. *Acta Crystallogr., Sect. E* **2006**, *62*, o3816–o3818.
- (25) Olovsson, I. A Low-Temperature Study of Some Simple Hydrogen-Bonded Structures. *Ark. Kemi* **1960**, *16*, 437–458.
- (26) Mishra, B. K.; Sathyamurthy, N. π – π Interaction in Pyridine. *J. Phys. Chem. A* **2005**, *109*, 6–8.
- (27) Khan, M.; Ahmad, A.; Ullah, M. F. Synthesis, Crystal Structure, Antimicrobial Activity and DNA-Binding of Hydrogen-Bonded Proton-Transfer Complex of 2,6-Diaminopyridine with Picric Acid. *J. Photochem. Photobiol. B* **2011**, *103*, 42–49.
- (28) Yu, G. 2,6-Diaminopyridinium Dihydrogen Phosphate. *Acta Crystallogr., Sect. E* **2012**, *68*, o2751–o2756.
- (29) Mahe, N.; Nicolai, B.; Allouchi, H.; Barrio, M.; Do, B.; Ceolin, R.; Tamarit, J. L.; Rietveld, I. B. Crystal Structure and Solid-State Properties of 3,4-Diaminopyridine Dihydrogen Phosphate and their Comparison with other Diaminopyridine Salts. *Cryst. Growth Des.* **2013**, *13*, 708–715.
- (30) Sheldrick, G. M. *SHELX-97*; University of Göttingen: Göttingen, Germany, 1997.
- (31) Wolff, S. K.; Grimwood, D. J.; McKinnon, J. J.; Jayatilaka, D.; Spackman, M. A. *Crystal Explorer*, version 2.1; University of Western Australia: Crawley, WA, Australia, 2007.
- (32) Spackman, M. A.; McKinnon, J. J. Fingerprinting Intermolecular Interactions in Molecular Crystals. *CrystEngComm* **2002**, *4*, 378–392.
- (33) Prakash, M. J.; Radhakrishnan, T. P. SHG Active Salts of 4-Nitrophenolate with H-Bonded Helical Formations: Structure-Directing Role of *ortho*-Aminopyridines. *Cryst. Growth Des.* **2005**, *5*, 721–725.
- (34) Allen, F. H. The Cambridge Structural Database: A Quarter of a Million Crystal Structures and Rising. *Acta Crystallogr., Sect. B* **2002**, *58*, 380–388.
- (35) Bruno, I. J.; Cole, J. C.; Kessler, M.; Luo, J.; Motherwell, W. D. S.; Purkis, L. H.; Smith, B. R.; Taylor, R.; Cooper, R. I.; Harris, S. E.; Orpen, A. G. Retrieval of Crystallographically-Derived Molecular Geometry Information. *J. Chem. Inf. Comput. Sci.* **2004**, *44*, 2133–2144.
- (36) Wuest, J. D. Molecular Solids: Co-Crystals Give Light a Tune-Up. *Nat. Chem.* **2012**, *4*, 74–75.
- (37) Hori, A.; Takatani, S.; Miyamoto, T. K.; Hasegawa, M. Luminescence from π – π Stacked Bipyridines through Arene–Perfluoroarene Interactions. *CrystEngComm* **2009**, *11*, 567–569.
- (38) Dai, X. P.; Hou, G. G.; Sun, J. F.; Lin, D.; Han, J. T. Synthesis, Structure and Luminescence of Novel 2D Co-Crystals based on Asymmetric 5-Substituted Pyrimidines and Isophthalic Acid: Alternate Arrangement and π – π Interactions. *J. Mol. Struct.* **2013**, *1035*, 203–208.

- (39) Muthu Prabhu, A. A.; Siva, S.; Sankaranarayanan, R. K.; Rajendiran, N. Intramolecular Proton Transfer Effects on 2,6-Diaminopyridine. *J. Fluoresc.* **2010**, *20*, 43–54.
- (40) Karpagam, J.; Sundaraganesan, N.; Kalaichelvan, S.; Sebastian, S. Anharmonic Vibrational Analysis of 3,4-Diaminopyridine and 3-Aminopyridine by Density Functional Theory Calculations. *Spectrochim. Acta, Part A* **2010**, *76*, 502–512.
- (41) John, C. J.; Amalanathan, M.; Twinkle, A. R.; Srinivasan, P.; Joe, I. H. Vibrational Spectra and First Order Hyperpolarizability Studies of Dimethyl Amino Pyridinium 4-Nitrophenolate 4-Nitrophenol. *Spectrochim. Acta, Part A* **2011**, *81*, 151–161.
- (42) Ahmed, A. B.; Feki, H.; Abid, Y.; Boughzala, H.; Minot, C.; Mlayah, A. Crystal Structure, Vibrational Spectra and Theoretical Studies of L-Histidinium Dihydrogen Phosphate–Phosphoric Acid. *J. Mol. Struct.* **2009**, *920*, 1–7.
- (43) Ilczyszyo, M. M.; Ratajczak, H.; Barnes, A. J. Polarized Infrared and Raman Spectra of Urea–Phosphoric Acid and Urea–Arsenic Acid Single Crystals. *J. Raman Spectrosc.* **1992**, *23*, 1–13.
- (44) Rudolph, W. W. Raman and Infrared Spectroscopic Investigations of Dilute Aqueous Phosphoric Acid Solutions. *Dalton Trans.* **2010**, *39*, 9642–9653.
- (45) Hachani, S.; Moine, B.; El-akrmi, A.; Ferid, M. Luminescent Properties of Some Ortho- and Pentaphosphates Doped with Gd³⁺–Eu³⁺: Potential Phosphors for Vacuum Ultraviolet Excitation. *Opt. Mater.* **2009**, *31*, 678–684.
- (46) Aitipamula, S.; Wong, A. B. H.; Chow, P. S.; Tan, R. B. H. Pharmaceutical Cocrystals of Ethenzamide: Structural, Solubility and Dissolution Studies. *CrystEngComm* **2012**, *14*, 8515–8524.
- (47) Barsky, I.; Bernstein, J.; Stephens, P. W.; Stone, K. H. The Study of the Polymorphic System of 2-Chloro-4-Nitrobenzoic Acid. *New J. Chem.* **2008**, *32*, 1747–1753.
- (48) Tommasini, M.; Castiglioni, C.; Del Zoppo, M.; Zerbi, G. Relationship between Infrared and Raman Intensities in Molecules with Polarized π Electrons. *J. Mol. Struct.* **1999**, *480*, 179–188.
- (49) Socrates, G. *Infrared and Raman Characteristic Group Frequencies*, 3rd ed.; John Wiley & Sons: Chichester, England, 2001.
- (50) Anto, P. L.; Anto, R. J.; Varghese, H. T.; Panicker, C. Y.; Philip, D. Vibrational Spectroscopic Studies and *ab Initio* Calculations of Phenyl Phosphate Disodium Salt. *J. Raman Spectrosc.* **2010**, *41*, 113–119.
- (51) Venkateswaran, C. S. The Raman Spectra of Ortho-Phosphoric Acid and Some Phosphates. *Proc. Indian. Acad. Sci.* **1935**, *3*, 25–30.
- (52) Conti, F.; Majerus, A.; Di Noto, V.; Korte, C.; Lehnert, W.; Stolten, D. Raman Study of the Polybenzimidazole–Phosphoric Acid Interactions in Membranes for Fuel Cells. *Phys. Chem. Chem. Phys.* **2012**, *14*, 10022–10026.
- (53) Krishnakumar, V.; Sivakumar, S.; Nagalakshmi, R.; Bhuvaneswari, S.; Rajaboopathi, M. Effect of Doping an Organic Molecule Ligand on TGS Single Crystals. *Spectrochim. Acta, Part A* **2008**, *71*, 480–485.
- (54) Karthick, T.; Balachandran, V.; Perumal, S.; Nataraj, A. Rotational Isomers, Vibrational Assignments, HOMO–LUMO, NLO Properties and Molecular Electrostatic Potential Surface of N-(2-Bromoethyl)phthalimide. *J. Mol. Struct.* **2011**, *1005*, 202–213.
- (55) Favini, G.; Gamba, A.; Bellobono, I. R. Ultra-Violet Absorption of Substituted Pyridines—I. Amino- and Nitropyridines. *Spectrochim. Acta, Part A* **1967**, *23*, 89–108.
- (56) Ultraviolet and Visible Spectrophotometry. <http://nsdl.niscair.res.in/jspui/handle/123456789/772> (accessed July 2014).
- (57) Hong, Y. N.; Lam, J. W. Y.; Tang, B. Z. Aggregation-Induced Emission. *Chem. Soc. Rev.* **2011**, *40*, 5361–5388.
- (58) Yuan, W. Z.; Lu, P.; Chen, S.; Lam, J. W. Y.; Wang, Z. M.; Liu, Y.; Kwok, H. S.; Ma, Y. G.; Tang, B. Z. Changing the Behavior of Chromophores from Aggregation-Caused Quenching to Aggregation-Induced Emission: Development of Highly Efficient Light Emitters in the Solid State. *Adv. Mater.* **2010**, *22*, 2159–2163.
- (59) Sudha, S.; Sundaraganesan, N.; Kurt, M.; Cinar, M.; Karabacak, M. FT-IR and FT-Raman Spectra, Vibrational Assignments, NBO Analysis and DFT Calculations of 2-Amino-4-Chlorobenzonitrile. *J. Mol. Struct.* **2011**, *985*, 148–156.
- (60) Kim, J. S.; Yang, S. C.; Park, H. J.; Bae, B. S. Photo-Curable Siloxane Hybrid Material Fabricated by a Thiolene Reaction of Sol-Gel Synthesized Oligosiloxanes. *Chem. Commun.* **2011**, *47*, 6051–6053.